Spectrally resolved femtosecond reflectivity relaxation dynamics in undoped spin-density wave 122-structure iron-based pnictides

A. Pogrebna,[1] N.Vujičić ,[1,2] T. Mertelj,[1] T. Borzda,[1] G. Cao,[3] Z. A. Xu,[3] J.-H. Chu,[4] I. R. Fisher,[4] and D. Mihailovic[1]

[1]*Complex Matter Deptartment, Jozef Stefan Institute, Jamova 39, Ljubljana, SI-1000, Ljubljana, Slovenia*

[2]*Institute of Physics, Bijenička 46, HR-10000 Zagreb, Croatia*

[3]*Department of Physics, Zhejiang University, Hangzhou 310027, People Republic of China*

[4]*Geballe Laboratory for Advanced Materials and Department of Applied Physics, Stanford University, Stanford, California 94305, USA*

(Received 24 February 2014; revised manuscript received 8 April 2014; published 24 April 2014)

We systematically investigate temperature- and spectrally dependent optical reflectivity dynamics in $A As_2Fe_2$, (A = Ba, Sr, and Eu), iron-based superconductors parent spin-density wave (SDW) compounds. Two different relaxation processes are identified. The behavior of the slower process, which is strongly sensitive to the magnetostructural transition, is analyzed in the framework of the relaxation-bottleneck model involving magnons. The results are compared to recent time-resolved angular photoemission results (TR-ARPES) and possible alternative assignment of the slower relaxation to the magnetostructural order parameter relaxation is discussed.

DOI: 10.1103/PhysRevB.89.165131 PACS number(s): 75.30.Fv, 78.47.jg, 74.70.Xa

I. INTRODUCTION

Time domain optical spectroscopy has been, among other spectroscopies, very instrumental in elucidating the nature of the superconducting and unusual normal states in novel superconductors and related materials by virtue of the fact that different components in the low-energy excitation spectrum could be distinguished by their lifetimes [1–13]. Unfortunately, the all-optical technique lacks the momentum resolution so assignments of the relaxation processes were indirect, based on model-predicted temperature and fluence dependencies [14–16]. Despite the indirect assignments no inconsistencies with the previous all-optical based results were found for the cuprates by the recent laser time-resolved angular-resolved-photoemission [17,18] experiments.

Most of the published all-optical time resolved experiments were performed using relatively narrowband spectrally unresolved probes. Since narrowband probes can be rather selective, probing only a limited subset of the relevant low-energy electronic states, and laser TR-ARPES suffers from surface sensitivity and limited momentum range, broadband spectrally resolved all-optical transient experiments are necessary to complement both probes and elucidate information about any additional relaxation processes, that might have been missed due to the limitations.

In the cuprates, a few such experiments have been performed [19–21] indicating, that there are no additional low-temperature relaxation processes to the ones previously observed by all-optical narrowband probes and associated with the pseudogap and the superconducting states [21]. In iron-based superconductors, to our best knowledge, no broad-band time-resolved spectroscopy data exist, except in the terahertz region [22]. Similarly to the cuprates, however, the narrowband all-optical time-resolved spectroscopy indicates a limited number of distinctive relaxation components [9,10,12,13,23].

The multiband nature of iron-based pnictides offers a possibility of additional photoexcited quasiparticle relaxation pathways that might remain undetected by the narrowband optical and laser TR-ARPES [24] probes. In the absence of broad-band time-resolved spectroscopy data in iron-based pnictides and in order to check about existence of additional processes, we therefore performed a systematic spectrally resolved visible broad-band probe transient-reflectivity study of the SDW state in three related undoped parent compounds $A Fe_2As_2$ (A-122) with A = Ba, Sr, and Eu.

Previously it was shown [23,25] that in the SDW state a single ∼1-ps relaxation component dominates the near-infrared narrowband optical response, while TR-ARPES experiments [24] indicate at least two distinct relaxation processes, with the longest relaxation time similar to the one observed in the optical response.

Our new broadband-probe results confirm previous near-infrared narrowband results and suggest the existence of another faster sub-200-fs relaxation component in addition to the previously reported slower one [23–25] for all three investigated compounds. The additional component is comparable or faster than the experimental temporal resolution of ∼200 fs and compatible with the fastest component measured by TR-ARPES [24]. The slower, previously observed, shows, differently from TR-ARPES, a divergentlike relaxation time at the respective magnetostructural transition temperatures.

The temperature dependencies of the optical-relaxation-transient amplitudes are analyzed and discussed in the framework of the relaxation bottleneck due to opening of the partial charge gap in the orthorhombic SDW state. An alternative assignment of the slower component to the SDW amplitude mode is also discussed in relation to the recent proposal for description of the transient optical reflectivity in the charge-density wave state [26].

II. EXPERIMENTAL

A. Samples

Single crystals of $EuFe_2As_2$ and $SrFe_2As_2$ were grown at Zhejiang University by a flux method, similar to a previous report [27]. Small Eu chunks and powders of Fe, As (Alfa Aesar, >99.9%) were mixed together in the molar ratio of Eu:Fe:As = 1:5:5 and sealed in an evacuated quartz ampoule. After heating the mixture up to 973 K for 24 hours, the obtained precursor was thoroughly ground before being loaded into an alumina crucible. The crucible was then sealed by arc welding

in a tube made of stainless steel under atmosphere of argon, and then heated up to 1573 K over 10 hours in a muffle furnace filled with argon. After holding at 1573 K for 5 hours, the furnace was cooled down to 1223 K at the rate of 5 K/h. followed by switching off the furnace. Large crystals with size up to $4 \times 4 \times 0.6$ mm^3 could be harvested.

The as-grown crystals were characterized by x-ray diffraction, which showed good crystallinity as well as single "122" phase. The exact composition of the crystals was determined by energy dispersive x-ray spectroscopy affiliated to a field-emission scanning electron microscope (FEI Model SIRION). The measurement precision was better than 5% for the elements measured. Single crystals of $BaFe_2As_2$ were also grown from from a self flux at Stanford University, and characterized as described previously [13,28]. In all three compounds, the onset of the magnetic SDW ordering is concurrent with the structural transition from tetragonal to orthorhombic symmetry at $T_{SDW} = 134$ K for Ba-122 [28], 190 K for Eu-122 [29], and 203 K for Sr-122 [29].

B. Optical setup

Measurements of probe-photon energy ($\hbar\omega_{pr}$) dependent photoinduced reflectivity $\Delta R/R$ were performed using a standard pump-probe technique. 50-fs optical pulses from a 250-kHz Ti:Al_2O_3 regenerative amplifier seeded with an Ti:Al_2O_3 oscillator were split in two mutually delayed parts. The pump photons with energy $\hbar\omega_P = 3.1$ eV were derived from one part by the standard frequency doubling in a BBO nonlinear crystal. The probe photons were obtained from a suprecontinuum generated in a 2.5-mm-thick Al_2O_3 plate by the second part. A short-pass Schott-glass filter was used to suppress the strong spectral density around 1.55 eV resulting in the useful spectral density within 1.65–2.55 eV band. The polarization of the probe photons with respect to the crystal was controlled by a broadband half waveplate and the beam was focused on the sample by a pair of achromatic lenses. The reflected probe beam was collimated, dispersed by a transmissive optical grating and focused on a 48-channel silicon PIN diode array. The array was connected to an in-house built 64-channel integrating analog to digital converter that was synchronized to the laser and synchronously drove an optical chopper inserted in the pump beam.

The supercontinuum pulse is chirped and about 2-ps long. The chirp enables recovery of the temporal resolution by spectrally resolved detection. The chirp was calibrated by determination of the zero delay as a function of the probe-photon energy from the data measured near the room T, where the relaxation dynamics is comparable [13,23] to the temporal resolution of the setup of $\sim 200 - 300$ fs. For Ba-122 and Eu-122, the chirp calibration was based on Ba-122 data measured at $T = 280$ K with an increased pump fluence to improve the signal to noise ratio. Sr-122 was measured in a separate run and has independent chirp calibration based on $T = 270$ K Sr-122 data.

The pump and probe beams were nearly perpendicular to the cleaved sample surface (001). The probe polarization was oriented with respect to the crystals to obtain the maximum/minimum amplitude of $\Delta R/R$ at low temperatures with the pump polarization at $\sim 45^\circ$ with respect to the probe. The pump beam diameters were, depending on experimental conditions, in a 100 μm range with a smaller probe beam diameter of ~ 50 μm.

Due to a smaller signal/noise ratio of the broadband setup with respect to the narrowband one, the pump fluences used were higher than in our previous narrowband work [13,23], in the ~ 50 μJ/cm^2 range. However, the linearity of the responses with respect to both, the pump and the probe fluences was checked to ensure that the experiments were performed in the weak excitation regime.

C. Overview of the experimental data set

In Fig. 1, we show temperature dependent $\Delta R/R$ in Eu-122 measured by narrowband 50-fs probe pulses at, $\hbar\omega_{pr} = 1.55$ eV, photon energy. A marked increase of $\Delta R/R$ transients amplitude is observed around the magnetostructural transition temperature upon cooling, consistent with previous reports in Sr-122 and Ba-122 [9,13,23]. Similarly as observed in Ba-122, the transients show a twofold in-plane rotational symmetry well above the tetragonal to orthorhombic magnetostructural transition at $T_{SDW} = 190$ K. In Fig. 2, the probe-photon energy dependence of $\Delta R/R$ at and above T_{SDW} is shown for the two orthogonal polarizations. In the absence of information about the orientation of the crystallographic axes, we denote the polarizations $\mathcal{P}^+$ and $\mathcal{P}^-$ according to the sign of the response at the lowest probe-photon energy. With increasing $\hbar\omega_{pr}$ the response for the $\mathcal{P}^+$ polarization changes sign at $\hbar\omega_{pr} \sim 2.35$ eV. The signal for the $\mathcal{P}^-$ polarization, on the other hand, changes sign at a slightly larger $\hbar\omega_{pr} \sim 2.5$ eV, almost at the edge of our experimental spectral range.

Similar behavior is observed in Sr-122 (see Fig. 3), where the zero crossing is slightly lower, at $\hbar\omega_{pr} \sim 2.23$ eV, for the $\mathcal{P}^+$ polarization and slightly higher, just at the edge of the spectral window, at $\hbar\omega_{pr} \sim 2.56$ eV, for the $\mathcal{P}^-$ polarization. In Ba-122, the signal is less anisotropic below T_{SDW} [13] so only the $\mathcal{P}^-$ polarization was measured, that shows no indication of the sign change below T_{SDW} as shown in Fig. 4. In all three samples, the spectral dependence of the transients does not change qualitatively through the transition.

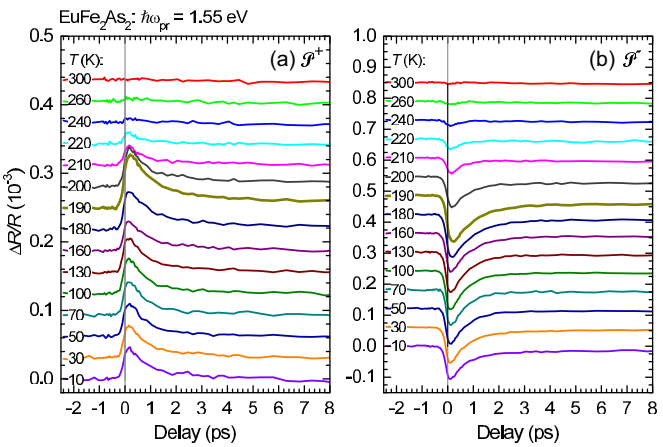

FIG. 1. (Color online) Photoinduced reflectivity transients at representative temperatures at $\mathcal{F} \simeq 10$ μJ/cm^2 and 3.1-eV pump-photon energy in $EuFe_2As_2$. Left and right panels correspond to $\mathcal{P}^+$ and $\mathcal{P}^-$ polarizations, respectively. The traces are vertically offset for clarity.

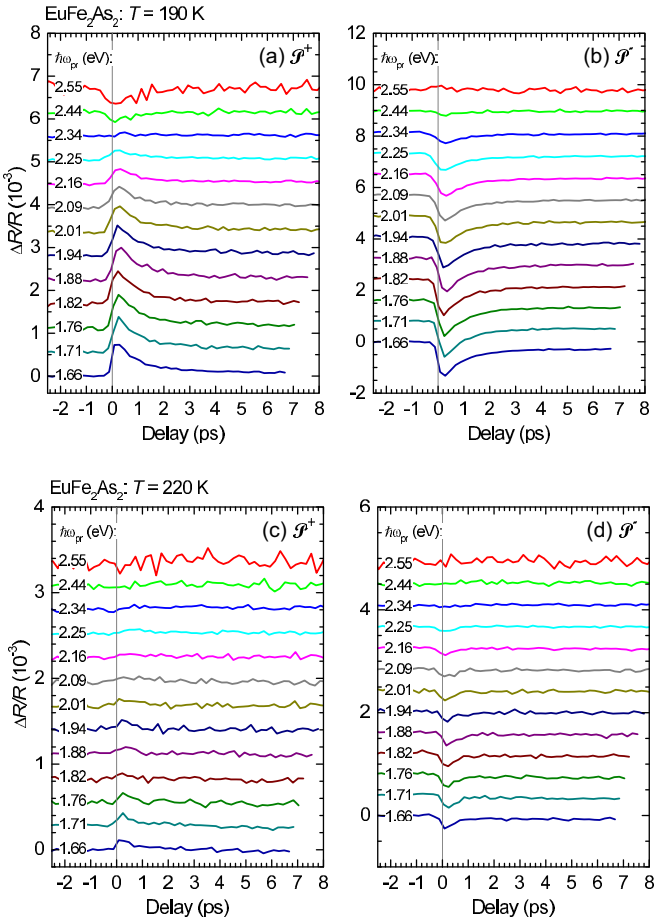

FIG. 2. (Color online) Photoinduced reflectivity transients in $EuFe_2As_2$ as a function of the probe-photon energy at T_{SDW}, (a) and (b), and above T_{SDW}, (c) and (d). (a), (c) and (b), (d) correspond to $\mathcal{P}^+$ and $\mathcal{P}^-$ polarizations, respectively. The traces are vertically offset for clarity.

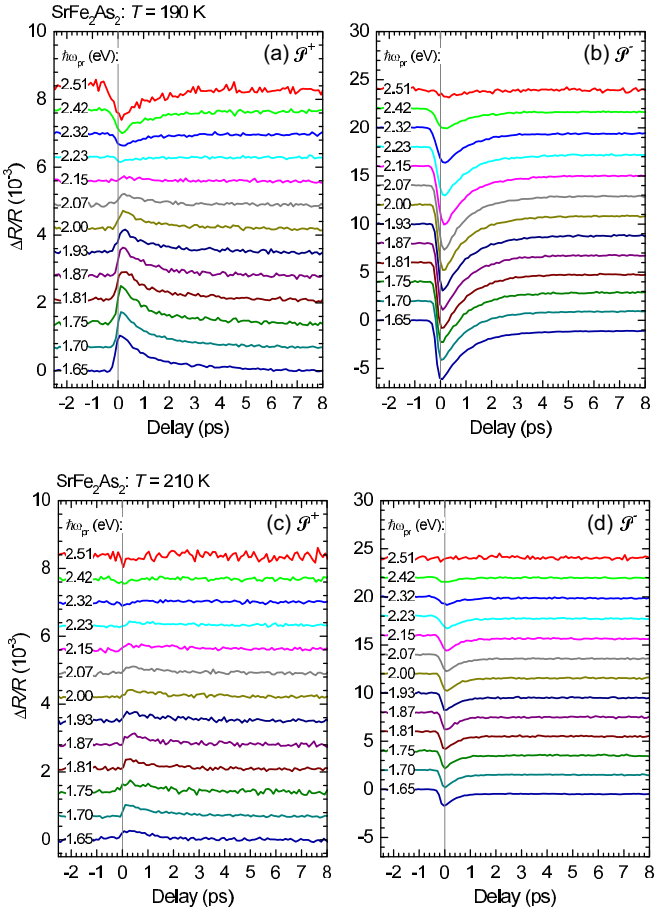

FIG. 3. (Color online) Photoinduced reflectivity transients in $SrFe_2As_2$ as a function of the probe-photon energy just below T_{SDW}, (a) and (b), and above T_{SDW}, (c) and (d). (a), (c) and (b), (d) correspond to $\mathcal{P}^+$ and $\mathcal{P}^-$ polarizations, respectively. The traces are vertically offset for clarity.

III. DATA ANALYSIS

A. Determination of independent components

The measured data points at each temperature can be arranged into a rectangular matrix and decomposed using the standard singular value decomposition (SVD) to obtain orthonormal eigenvectors describing the data:

$$\frac{\Delta R(\omega_{\mathrm{pr},i},t_j)}{R(\omega_{\mathrm{pr},i})} = \sum w_k u_{ik} v_{jk} = \sum A_k(\hbar\omega_{\mathrm{pr},i}) r_k(t_j). \quad (1)$$

Here, w_k, u_{ik}, and v_{jk} are the singular values (SV), the left singular eigenvectors and the right singular eigenvectors, respectively. With the above matrix arrangement we define the SVD spectral weights (SW) as weighted left singular eigenvectors $A_k(\omega_{\mathrm{pr},i}) = w_k u_{ik}$, while the right singular eigenvectors correspond to the orthonormal temporal eigenvectors (TEv): $r_k(t_j) = v_{jk}$.

In Fig. 5, we plot a few most significant TEv for each sample at temperatures just below T_{SDW} [31]. It is obvious that for each sample only the three most significant TEv contain most of the coherent response, while the rest represent noise only. Some spikes observed near the zero delay in less significant TEvs contribute very little and can not be reliably assigned as intrinsic due to the possible chirp-calibration-error induced artifacts.

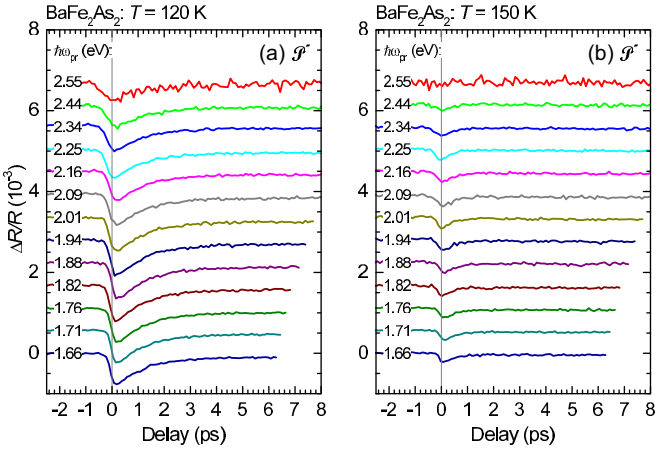

FIG. 4. (Color online) Photoinduced reflectivity transients in $BaFe_2As_2$ as a function of the probe-photon energy just below and just above T_{SDW} (a) and (b), respectively. The traces are vertically offset for clarity.

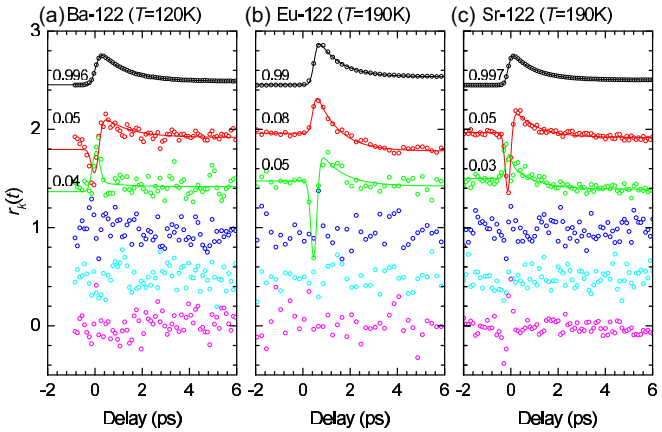

FIG. 5. (Color online) A few temporal eigenvectors with the highest singular values near T_{SDW}. The lines are exponential fits (2) for the three most significant temporal eigenvectors. The numerical labels are the normalized singular values $w_k/\sqrt{\sum w_l^2}$. The traces are vertically shifted for clarity.

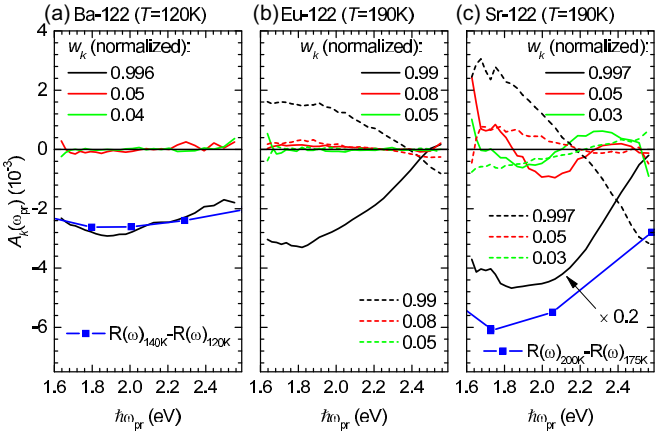

FIG. 7. (Color online) Spectral dependence of the three most significant SVD temporal-eigenvectors weights just below respective T_{SDW}. The numerical labels are normalized singular values. The thermal reflectivity difference from Ref. [30] for Ba-122 in Sr-122 is shown for comparison.

Since any errors in chirp calibration can lead to spurious components also for the more significant TEvs we checked for the presence of subpicosecond transients in the near-room-T SVD. From Fig. 6, it can be seen that near the room T the subpicosecond component is well contained in a single TEv. In Ba-122 and Eu-122, however, some chirp-calibration-error induced contribution can not be completely excluded due to the small SW of the second and third TEv.

SW corresponding to the three most significant TEv are shown in Fig. 7. The TEv with the largest SV clearly dominates the spectral response in all compounds. In Ba-122 and Eu-122, the SW of the next two TEv are near the noise level while in Sr-122 they are almost comparable to the first TEv SW for the $\mathcal{P}^+$ polarization. The spectral dependence of the most intensive component SW is very similar to the static reflectivity change when crossing the magnetostructural transition [30] in Ba-122. In Sr-122, however, the similarity is only in the peak position at ∼1.7 eV with a large difference between the positions of the zero crossings.

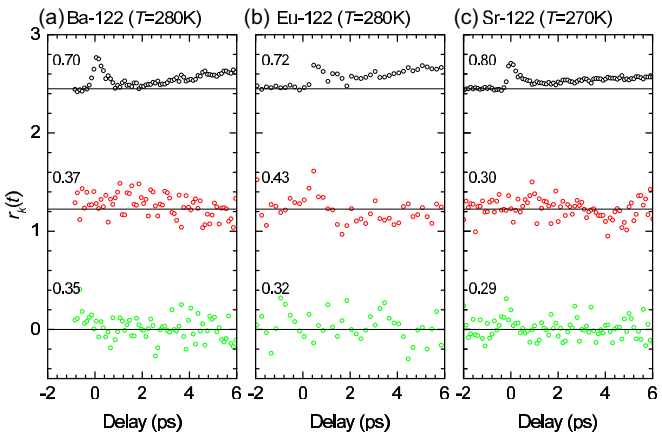

FIG. 6. (Color online) The three temporal eigenvectors with the highest singular values near the room temperature. The numerical labels are the normalized singular values $w_k/\sqrt{\sum w_l^2}$. The traces are vertically shifted for clarity.

The three largest SV TEv can be rather well fit by a double exponential relaxation model with a finite risetime/resolution and a finite long delay value (see Fig. 5):

$$r_k(t) = \sum_{m\in\{A,B\}} \frac{A_{m,k}}{2} e^{-\frac{t-t_0}{\tau_m}} \operatorname{erfc}\left[\frac{\sigma^2 - 4(t-t_0)\tau_m}{2\sqrt{2}\sigma\tau_m}\right] + \frac{A_{C,k}}{2} \operatorname{erfc}\left[-\frac{\sqrt{2}(t-t_0)}{\sigma}\right]. \quad (2)$$

Here, the rise-time/resolution parameter σ and relaxation times τ_m are shared among the three TEv, while the amplitudes $A_{l,k}$ are kept independent.

The fits yield virtually T-independent σ of 200–300 fs shown in Fig. 8 indicating that it corresponds to the instrumental resolution [32]. One of the relaxation times, τ_A, was

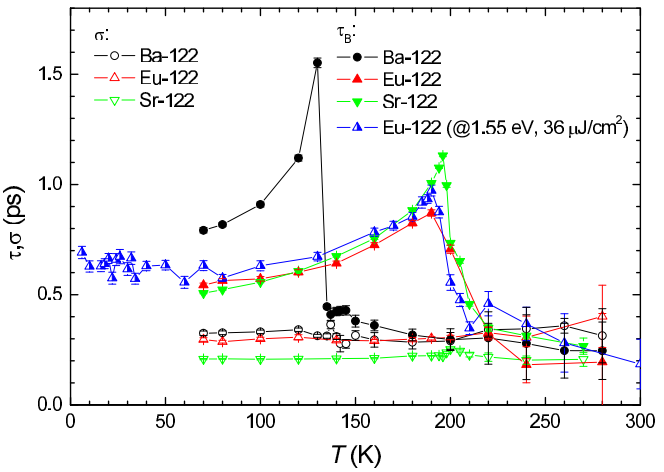

FIG. 8. (Color online) The rise-time/resolution parameter and the longest relaxation time, τ_B, as a function of T. The shortest relaxation time, τ_A, is shorter than σ, so it was kept constant at 50 fs for all fits. The 1.55-eV probe result in Eu-122 is also shown for comparison.

found significantly shorter than σ so it was kept constant at 50 fs for all fits. The second relaxation time τ_B shows a marked T dependence with a divergent like behavior at T_{SDW}. In Ba-122, it sharply drops above T_{SDW}, while in Eu-122 and Sr-122 the drop is somewhat less steep. At T significantly above T_{SDW} it becomes comparable to the experimental temporal resolution.

B. Bottleneck model fits

To analyze the anisotropic T dependence of the $\Delta R/R$ amplitude, we start with the general form of equation that describes the photoinduced reflectivity change due to the presence of photoexcited carriers for a pair of bands [13]:

$$\Delta R_{\alpha,\beta} \propto \int d^3k[|M_{\alpha,\beta}(\mathbf{k})|^2 \Delta f_\alpha(\mathbf{k}) \times g(\epsilon_\beta(\mathbf{k}) - \epsilon_\alpha(\mathbf{k}) - \hbar\omega_{pr})]. \quad (3)$$

Here, $M_{\alpha,\beta}$ is the effective probe-polarization dependent optical-dipole matrix element between an initial band, α, and a final band, β, $\Delta f_\alpha(\mathbf{k})$ the photoexcited change of the quasiparticle distribution function in the initial band, $g(\epsilon)$ the effective transition line shape and $\hbar\omega_{pr}$ the probe-photon energy. For simplicity, we assumed that the energy of the final band is far from the Fermi energy, $|\epsilon_\beta(\mathbf{k}) - \epsilon_F| \sim \hbar\omega_{probe} \gg k_B T$, so $\Delta f_\beta(\mathbf{k})$ can be neglected after the fast initial relaxation of the ultrahot carriers.

The integral (3) selectively samples $\Delta f_\alpha(\mathbf{k})$ in different regions of the k-space depending on the probe polarization and photon energy. Due to contributions of several optical transitions with finite effective linewidths it is usually assumed that (3) smoothly samples over the relevant energy range in the vicinity of the Fermi energy and ΔR can be approximated by the total photoexcited carrier density, $\Delta R = \gamma n_{pe}$ [14,33], and any change of ΔR upon change of external parameters (T for example) is attributed to the change of n_{pe}, while the proportionality factor γ is assumed to be constant.

In AFe_2As_2, however, a complex band structure reorganization, with bands shifting by as much as 80 meV, has been observed below T_{SDW} [34]. These shifts can significantly modify the sampling region of the integral (3) and violate

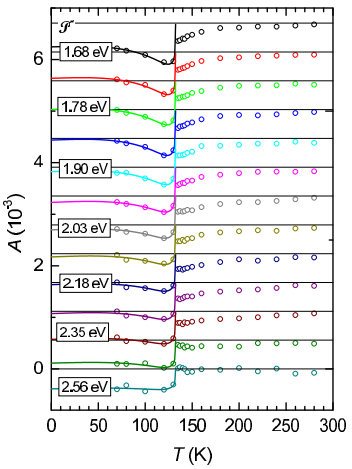

FIG. 9. (Color online) The amplitude of the $\Delta R/R$ transients in $BaFe_2As_2$ as a function of T. The thin lines are the bottleneck-model (4) fits discussed in text. The traces are vertically offset for clarity.

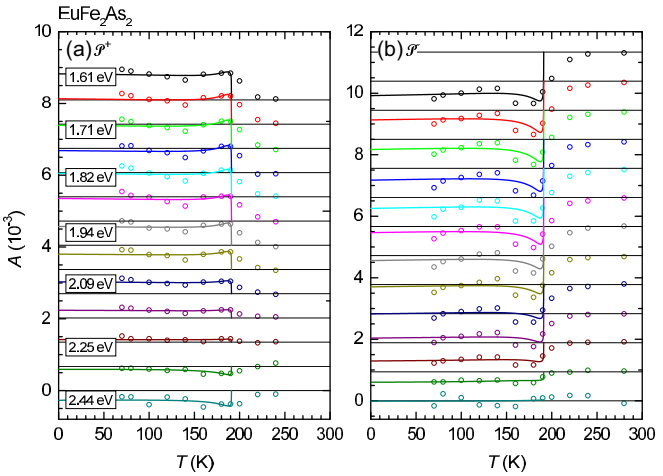

FIG. 10. (Color online) The amplitude of the $\Delta R/R$ transients in $EuFe_2As_2$ as a function of T. (a) and (b) correspond to $\mathcal{P}^+$ and $\mathcal{P}^-$ polarizations, respectively. The thin lines are the bottleneck-model (4) fits discussed in text. The traces are vertically offset for clarity.

the assumption of a constant γ. To take this into account, we therefore assume that γ is temperature dependent and expand it in terms of an order parameter. The order parameter can be associated with the opening of a partial T-dependent charge gap $\Delta(T)$ upon the Fermi surface reconstruction below T_{SDW} [35]. Assuming a complex BCS-like order parameter with the magnitude $\Delta(T)$, we expand γ to the lowest symmetry-allowed order and obtain [13]

$$\Delta R = \left[\gamma_0 + \eta \frac{\Delta^2(T)}{\Delta^2(0)}\right] n_{pe}. \quad (4)$$

To describe the T dependence of n_{pe}, we use the bottleneck model from Kabanov *et al.* [14],

$$n_{pe} \propto \frac{1}{\left\{\left(\frac{2\Delta(T)}{k_B T_{SDW}} + \frac{T}{T_{SDW}}\right)\left[1 + g_{ph}\sqrt{\frac{k_B T}{\Delta(T)}}\exp\left(-\frac{\Delta(T)}{k_B T}\right)\right]\right\}}, \quad (5)$$

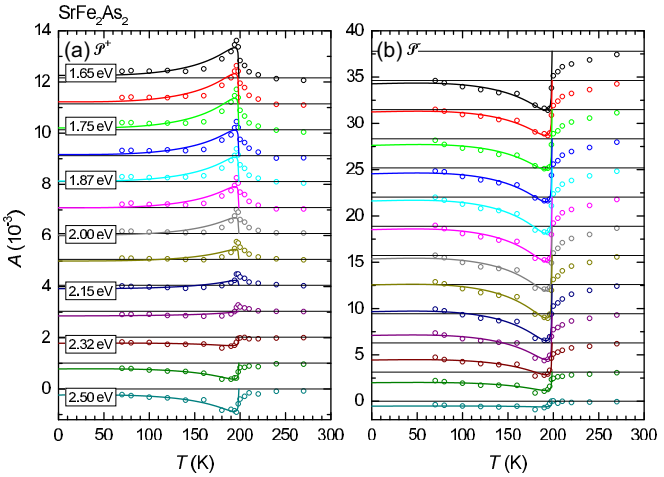

FIG. 11. (Color online) The amplitude of the $\Delta R/R$ transients in $SrFe_2As_2$ as a function of T. (a) and (b) correspond to $\mathcal{P}^+$ and $\mathcal{P}^-$ polarizations, respectively. The thin lines are the bottleneck-model (4) fits discussed in text. The traces are vertically offset for clarity.

TABLE I. Charge gap magnitudes and the relative effective number of involved bosons as obtained from the fits of (4) to the data shown in Figs. 9–11. The results of a fit to the data in $YBa_2Cu_3O_{7-\delta}$ superconductor [1] ($T_c = 93$ K) and the larger-gap values obtained from the optical conductivity (indicated with "*") are shown for comparison.

Sample	$2\Delta(0)/k_B T_{SDW}$	g_{ph}
Ba-122	8 ± 6	3.2 ± 1.1
Eu-122	13 ± 8	2.8 ± 1.4
Sr-122	8 ± 3	2.7 ± 0.8
$YBa_2Cu_3O_{7-\delta}$ [1]	10	~60
*Ba-122	7.7 [30], ~9 [38]	···
*Sr-122	8.7 [30], ~9 [38]	···
*Eu-122	5.6 [39]	···

where g_{ph} represents the relative effective number of the involved boson degrees of freedom. Using the BCS temperature dependent gap, we can obtain a good fit [36] of Eq. (4) to the $\Delta R/R$ amplitude [37] for both probe polarizations (see Figs. 9–12). The relative gap magnitudes are consistent (see Table I) with previously reported values [13,23] and the larger of the two gaps observed in the optical conductivity [30,38], with a somewhat bigger discrepancy for Eu-122 [39].

IV. DISCUSSION

The bottleneck model [5] is based on the assumption that on a certain timescale a quasi-equilibrium is achieved between a gaped quasiparticle population and a boson population with characteristic energy of $\hbar\omega = 2\Delta(T)$. This assumption is valid when the energy relaxation is sufficiently slow, even if the system is not fully gaped as is the case of the investigated SDW iron pnictides, that remain metallic below T_{SDW}. The quasiequilibrium is achieved on a timescale of ~200 fs and the energy relaxation time is in the 0.5–1.5 ps range. Based on the room-T relaxation times [13,23], where the relaxation is governed by the electron phonon interaction [19,40], the rise time is long enough for establishing a quasiequilibrium between the quasiparticle and high-frequency phonon populations. On the other hand, the characteristic boson energies

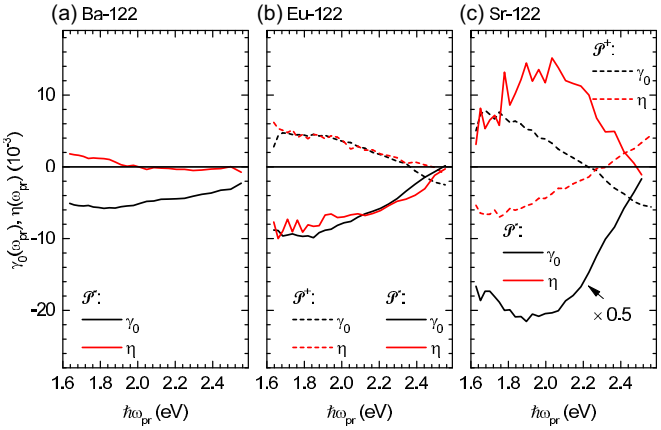

FIG. 12. (Color online) Spectral dependence of the fit amplitudes for all three samples.

obtained from the fits are in the range ~100–200 meV and significantly exceed the maximum phonon energy, <50 meV [41]. The phonon bottleneck is therefore *not consistent* with the fit results, except near the transition, where $\Delta(T)$ is smaller.

Another possible boson reservoir are antiferromagnetic magnons with maximum energies exceeding ~200 meV [42–44]. The number of magnon degrees of freedom is, however, much smaller than the number of phonon degrees of freedom [45] and should be reflected in g_{ph}. Indeed, the obtained values of g_{ph} are significantly smaller than in the cuprate superconductor $YBa_2Cu_3O_{7-\delta}$ (see Table I) [46], where the phonon bottleneck was clearly established.

As for the phonons, the quasiparticle-magnon interaction timescale needs to be fast enough for establishing the quasiequilibrium. For itinerant magnetic systems, it has been shown [47] that the demagnetization upon photoexcitation appears on a few-hundred femtoseconds time scale. Moreover, the quasiparticle-magnon interaction is determined by the spin-orbit coupling, which is large (~0.4 eV) for As-p orbitals, which hybridize with Fe-d orbitals [48] and increase the coupling. In A-122, hence the quasiparticle-magnon interaction timescale is expected to be short enough to be compatible with the magnon bottleneck mechanism.

The bottleneck model with magnons therefore consistently describes the data including the divergentlike increase [14] of τ_B at the magnetostructural transition and the obtained gap parameters are consistent with results obtained by means of the steady-state optical spectroscopy [30,38,39].

Comparing our data with the TR-ARPES results in Eu-122 [24] reveals agreement between the relaxation time of the resolution-limited fast component observed in our case and the T-dependent hole relaxation time of ~200–300 fs observed by TR-ARPES. A similar fast component was observed also in Co doped Ba-122 and Sm(Fe,Co)AsO by means of an all-optical narrowband probe [13,49]. We should note, however, that in Ba-122 and Eu-122 the magnitude of this component is very small and could be affected by the chirp-calibration errors.

Contrary, the T-dependent relaxation-time of the dominant slower component observed in our case differs from the slower TR-ARPES electron-relaxation time beyond the combined error bars of the experiments. While the low-T optical value of 650 fs is just slightly smaller than the TR-ARPES value of 800 fs, at T_{SDW}, the optical relaxation time shows a clear divergentlike behavior, which is absent in the TR-ARPES data. This indicates that either (i) the optical probe and TR-ARPES probe detect different relaxation processes or (ii) there are some unidentified surface effects that influence the relaxation near the surface probed by TR-ARPES preventing divergence. Since more systematic TR-ARPES investigations are needed to clarify possibility (ii) let us focus on possibility (i).

The photoinduced dielectric constant changes captured in Eq. (3) and taken into account in the bottleneck model are limited to the change of the nonequilibrium quasiparticle distribution function and neglect any change in $\epsilon(\mathbf{k})$ or the matrix elements. In collectively ordered systems such are density waves, however, the collective degrees of freedom can be significantly perturbed by the photoexcitation affecting both $\epsilon(\mathbf{k})$ and matrix elements. It was proposed recently [26,50] that the relaxation dynamics in charge-density waves can be described by coupled dynamics of an overdamped electronic amplitude mode and

phonon modes, without directly invoking the photoinduced-quasiparticles absorption scenario. In SDW systems, a similar overdamped Raman active amplitude mode was predicted [51,52], but, to our best knowledge, never observed.

Despite the fact that the bottleneck relaxation model discussed above describes the data below T_{SDW} rather consistently in a broad frequency range, there exists a possibility that the observed optical relaxation is due to the order parameter relaxation, the SDW *amplitude mode*. Indeed, the gap dynamics from TR-ARPES [24] shows 100–200-fs rise time and a subpicosecond decay consistent with the slower optical relaxation timescales. Moreover, the transient optical response shows a dominant single-component relaxation over a broad spectral range with a spectral dependence (Fig. 7) similar to the equilibrium phase-transition-induced reflectivity change [30,53] suggesting the transient order-parameter modulation origin of the optical response. The divergent behavior of the relaxation time near T_{SDW} is also consistent with the critical slowing down of the amplitude mode at the transition.

Above T_{SDW}, the spectral signature of the response that remains and is clearly breaking the tetragonal symmetry, is similar as in the SDW state. It was previously assigned [13,49] to the bottleneck due to the normal-state pseudogap and related to the nematic fluctuations. However, the same reasoning as above can be applied and assign it to the fluctuations of the magnetostructural order parameter.

The two alternative origins of the optical transient response, based on the microscopic nonequilibrium quasiparticle distribution function $\Delta f(\mathbf{k})$ in Eq. (3) on one hand, and a macroscopic order parameter on the other, are, however, not completely independent nor exclusive. In a BCS-like scenario the order parameter is directly related to the quasiparticle distribution function through the gap equation. Provided that the condensate dynamics is faster than the kinetics of $\Delta f(\mathbf{k})$, the time evolution of the order parameter is direcly governed by the $\Delta f(\mathbf{k})$ kinetics [54].

In the SDW state, the characteristic frequency of the pure electronic SDW amplitude mode is predicted [51] to be $2\Delta/\hbar$. Taking $2\Delta \sim 200$ meV would lead to ~3-fs time scale, which is much faster than the observed relaxation time. This would suggest that, irrespective of the origin of the optical coupling, the relaxation dynamics is governed by the bottleneck physics.

In the iron-based pnictides, however, the SDW order is clearly related to the structural transition, so it would not be surprising if the amplitude mode effective mass was renormalized due to coupling with the lattice, just like in charge density wave systems. In such case, the dynamics in the presence of a bottleneck is more complicated, leading to at least two distinct relaxation timescales, related to the bottleneck relaxation and the magnetostructural order parameter relaxation. In the absence of a bottleneck, however, a single magnetostructural order parameter relaxation timescale is expected.

Assuming that the fast component in our data corresponds to the relaxation at the ungapped parts of the Fermi surface, as suggested by Rettig *et al.* [24], the presence of the single-component exponential slower relaxation is compatible with either the pure bottleneck-driven dynamics with a fast amplitude mode dynamics or the complete absence of any bottleneck with slow pure magnetostructural order parameter dynamics.

By taking into account the bottlenecklike amplitude T dependencies and the indication of a fast initial suppression of the gap upon photoexcitation by TR-ARPES [24], the experimental data are in favor of the pure bottleneck-driven dynamics with the fast amplitude mode dynamics. The difference in the relaxation time behavior near the transition between optics and TR-ARPES could then be attributed to surface effects.

The process responsible for the modulation of the dielectric constant, however, can be a combination of the direct photoinduced absorption given by Eq. (3) and the indirect coupling through the order parameter modulation of $\epsilon(\mathbf{k})$ and matrix elements, as suggested by the similarity of the spectral dispersions between the transient photoinduced and the static phase-transition-induced [30] reflectivity changes.

V. SUMMARY AND CONCLUSIONS

A systematic all-optical spectrally resolved transient reflectivity study in AFe_2As_2 is presented for the first time. Two distinct relaxation components are identified.

(i) A fast one, previously unobserved by the near-infrared narrowband probe, which is faster or similar to the experimental temporal resolution of ~200 fs, is consistent with recent TR-ARPES [24] results and could be associated with relaxation at the Fermi surface.

(ii) The slower one on the timescale of 0.6–1.5 ps, observed previously by the near-infrared narrowband probe, with strong sensitivity to the magnetostructural transition, contrary to TR-ARPES, slows down near the magnetostructural transition. It can be well quantitatively described in a *broad spectral range* by a bottleneck model, with zero temperature gap magnitudes $2\Delta(0)/T_{SDW} \sim 8$, which are consistent with steady-state optical spectroscopy results. The bottleneck-model fits and the magnitude of the gap suggest that magnons play the role of the bottleneck bosons. An alternative assignment of the response to the SDW magnetostructural order-parameter amplitude mode dynamics was also discussed, however, the present experimental data are in favor of the pure bottleneck-driven dynamics.

ACKNOWLEDGMENTS

Work at Jozef Stefan Institute was supported by ARRS (Grant No. P1-0040) and ERC grant *Trajectory*. Work at Zhejiang University was supported by the National Science Foundation of China. We would also like to thank V. Kabanov for comments and fruitful discussions.

[1] J. Demsar, B. Podobnik, V. V. Kabanov, T. Wolf, and D. Mihailovic, Phys. Rev. Lett. **82**, 4918 (1999).

[2] R. Kaindl, M. Woerner, T. Elsaesser, D. Smith, J. Ryan, G. Farnan, M. McCurry, and D. Walmsley, Science **287**, 470 (2000).

[3] R. D. Averitt, G. Rodriguez, A. I. Lobad, J. L. W. Siders, S. A. Trugman, and A. J. Taylor, Phys. Rev. B **63**, 140502 (2001).

[4] G. P. Segre, N. Gedik, J. Orenstein, D. A. Bonn, R. Liang, and W. N. Hardy, Phys. Rev. Lett. **88**, 137001 (2002).

[5] P. Kusar, J. Demsar, D. Mihailovic, and S. Sugai, Phys. Rev. B **72**, 014544 (2005).

[6] E. E. M. Chia, J.-X. Zhu, H. J. Lee, N. Hur, N. O. Moreno, E. D. Bauer, T. Durakiewicz, R. D. Averitt, J. L. Sarrao, and A. J. Taylor, Phys. Rev. B **74**, 140409 (2006).

[7] Y. H. Liu, Y. Toda, K. Shimatake, N. Momono, M. Oda, and M. Ido, Phys. Rev. Lett. **101**, 137003 (2008).

[8] C. Ning, W. Yan-Feng, Z. Ji-Min, Z. Shi-Ping, Y. Qian-Sheng, Z. Zhi-Guo, and F. Pan-Ming, Chin. Phys. Lett. **25**, 2257 (2008).

[9] E. E. M. Chia, D. Talbayev, J.-X. Zhu, H. Q. Yuan, T. Park, J. D. Thompson, C. Panagopoulos, G. F. Chen, J. L. Luo, N. L. Wang, and A. J. Taylor, Phys. Rev. Lett. **104**, 027003 (2010).

[10] D. H. Torchinsky, G. F. Chen, J. L. Luo, N. L. Wang, and N. Gedik, Phys. Rev. Lett. **105**, 027005 (2010).

[11] G. Coslovich, C. Giannetti, F. Cilento, S. Dal Conte, G. Ferrini, P. Galinetto, M. Greven, H. Eisaki, M. Raichle, R. Liang, A. Damascelli, and F. Parmigiani, Phys. Rev. B **83**, 064519 (2011).

[12] T. Mertelj, V. V. Kabanov, C. Gadermaier, N. D. Zhigadlo, S. Katrych, J. Karpinski, and D. Mihailovic, Phys. Rev. Lett. **102**, 117002 (2009).

[13] L. Stojchevska, T. Mertelj, J.-H. Chu, I. R. Fisher, and D. Mihailovic, Phys. Rev. B **86**, 024519 (2012).

[14] V. V. Kabanov, J. Demsar, B. Podobnik, and D. Mihailovic, Phys. Rev. B **59**, 1497 (1999).

[15] J. Demsar, R. D. Averitt, A. J. Taylor, V. V. Kabanov, W. N. Kang, H. J. Kim, E. M. Choi, and S. I. Lee, Phys. Rev. Lett. **91**, 267002 (2003).

[16] N. Gedik, P. Blake, R. C. Spitzer, J. Orenstein, R. Liang, D. A. Bonn, and W. N. Hardy, Phys. Rev. B **70**, 014504 (2004).

[17] R. Cortés, L. Rettig, Y. Yoshida, H. Eisaki, M. Wolf, and U. Bovensiepen, Phys. Rev. Lett. **107**, 097002 (2011).

[18] C. L. Smallwood, J. P. Hinton, C. Jozwiak, W. Zhang, J. D. Koralek, H. Eisaki, D.-H. Lee, J. Orenstein, and A. Lanzara, Science **336**, 1137 (2012).

[19] C. Gadermaier, A. S. Alexandrov, V. V. Kabanov, P. Kusar, T. Mertelj, X. Yao, C. Manzoni, D. Brida, G. Cerullo, and D. Mihailovic, Phys. Rev. Lett. **105**, 257001 (2010).

[20] C. Giannetti, F. Cilento, S. Dal Conte, G. Coslovich, G. Ferrini, H. Molegraaf, M. Raichle, R. Liang, H. Eisaki, M. Greven *et al.*, Nat. Commun. **2**, 353 (2011).

[21] G. Coslovich, C. Giannetti, F. Cilento, S. Dal Conte, T. Abebaw, D. Bossini, G. Ferrini, H. Eisaki, M. Greven, A. Damascelli, and F. Parmigiani, Phys. Rev. Lett. **110**, 107003 (2013).

[22] K. W. Kim, A. Pashkin, H. Schäfer, M. Beyer, M. Porer, T. Wolf, C. Bernhard, J. Demsar, R. Huber, and A. Leitenstorfer, Nat. Mater. **11**, 497 (2012).

[23] L. Stojchevska, P. Kusar, T. Mertelj, V. Kabanov, X. Lin, G. Cao, Z. Xu, and D. Mihailovic, Phys. Rev. B **82**, 012505 (2010).

[24] L. Rettig, R. Cortés, S. Thirupathaiah, P. Gegenwart, H. S. Jeevan, M. Wolf, J. Fink, and U. Bovensiepen, Phys. Rev. Lett. **108**, 097002 (2012).

[25] T. Mertelj, P. Kusar, V. V. Kabanov, L. Stojchevska, N. D. Zhigadlo, S. Katrych, Z. Bukowski, J. Karpinski, S. Weyeneth, and D. Mihailovic, Phys. Rev. B **81**, 224504 (2010).

[26] H. Schäfer, V. V. Kabanov, M. Beyer, K. Biljakovic, and J. Demsar, Phys. Rev. Lett. **105**, 066402 (2010).

[27] W.-H. Jiao, Q. Tao, J.-K. Bao, Y.-L. Sun, C.-M. Feng, Z.-A. Xu, I. Nowik, I. Felner, and G.-H. Cao, Europhys. Lett. **95**, 67007 (2011).

[28] J.-H. Chu, J. G. Analytis, C. Kucharczyk, and I. R. Fisher, Phys. Rev. B **79**, 014506 (2009).

[29] M. Tegel, M. Rotter, V. Weiß, F. M. Schappacher, R. Pöttgen, and D. Johrendt, J. Phys. Condens. Matter **20**, 452201 (2008).

[30] A. Charnukha, D. Pröpper, T. I. Larkin, D. L. Sun, Z. W. Li, C. T. Lin, T. Wolf, B. Keimer, and A. V. Boris, Phys. Rev. B **88**, 184511 (2013).

[31] For Sr-122 and Eu-122, we performed SVD decomposition joining together the data for both polarizations at each T.

[32] Somewhat larger σ in Ba-122 and Eu-122 might be attributed to a slightly worse chirp compensation.

[33] D. Dvorsek, V. V. Kabanov, J. Demsar, S. M. Kazakov, J. Karpinski, and D. Mihailovic, Phys. Rev. B **66**, 020510 (2002).

[34] M. Yi, D. Lu, J.-H. Chu, J. G. Analytis, A. P. Sorini, A. F. Kemper, B. Moritz, S.-K. Mo, R. G. Moore, M. Hashimoto, W.-S. Lee, Z. Hussain, T. P. Devereaux, I. R. Fisher, and Z.-X. Shen, Proc. Natl. Acad. Sci. USA **108**, 6878 (2011).

[35] J. G. Analytis, R. D. McDonald, J.-H. Chu, S. C. Riggs, A. F. Bangura, C. Kucharczyk, M. Johannes, and I. R. Fisher, Phys. Rev. B **80**, 064507 (2009).

[36] For the fits T_{SDW} was fixed. The BCS gap magnitude $\Delta(0)$ and g_{ph} were linked between all probe-photon energies, while γ_0 and η were kept independent.

[37] The amplitude of the transients was determined by fitting a parabola to the extremum of the transient at each probe-photon energy and temperature.

[38] W. Z. Hu, J. Dong, G. Li, Z. Li, P. Zheng, G. F. Chen, J. L. Luo, and N. L. Wang, Phys. Rev. Lett. **101**, 257005 (2008).

[39] D. Wu, N. Barišić, N. Drichko, S. Kaiser, A. Faridian, M. Dressel, S. Jiang, Z. Ren, L. J. Li, G. H. Cao, Z. A. Xu, H. S. Jeevan, and P. Gegenwart, Phys. Rev. B **79**, 155103 (2009).

[40] C. Gadermaier, V. Kabanov, A. Alexandrov, L. Stojchevska, T. Mertelj, C. Manzoni, G. Cerullo, N. Zhigadlo, J. Karpinski, Y. Cai *et al.*, Phys. Rev. X **4**, 011056 (2014).

[41] M. Zbiri, R. Mittal, S. Rols, Y. Su, Y. Xiao, H. Schober, S. L. Chaplot, M. R. Johnson, T. Chatterji, Y. Inoue, S. Matsuishi, H. Hosono, and T. Brueckel, J. Phys. Condens. Matter **22**, 315701 (2010).

[42] R. A. Ewings, T. G. Perring, R. I. Bewley, T. Guidi, M. J. Pitcher, D. R. Parker, S. J. Clarke, and A. T. Boothroyd, Phys. Rev. B **78**, 220501 (2008).

[43] R. A. Ewings, T. G. Perring, J. Gillett, S. D. Das, S. E. Sebastian, A. E. Taylor, T. Guidi, and A. T. Boothroyd, Phys. Rev. B **83**, 214519 (2011).

[44] S. Sugai, Y. Mizuno, R. Watanabe, T. Kawaguchi, K. Takenaka, H. Ikuta, K. Kiho, M. Nakajima, C. Lee, A. Iyo, H. Eisaki, and S. Uchida, J. Supercond. Novel Magn. **26**, 1179 (2013).

[45] There are 27 optical phonon branches contrary to two spin branches in the doubly folded [55] magnetic unit cell.

[46] We have chosen $YBa_2Cu_3O_{7-\delta}$, for example, but the values are similar in other cuprate superconductors [5].

[47] A. Kirilyuk, A. V. Kimel, and T. Rasing, Rev. Mod. Phys. **82**, 2731 (2010).

[48] J. Wu, P. Phillips, and A. H. Castro Neto, Phys. Rev. Lett. **101**, 126401 (2008).
[49] T. Mertelj, L. Stojchevska, N. D. Zhigadlo, J. Karpinski, and D. Mihailovic, Phys. Rev. B **87**, 174525 (2013).
[50] H. Schaefer, V. V. Kabanov, and J. Demsar, Phys. Rev. B **89**, 045106 (2014).
[51] G. Psaltakis, Solid State Commun. **51**, 535 (1984).
[52] G. Grüner, Rev. Mod. Phys. **66**, 1 (1994).
[53] Since the transition-induced reflectivity change would be hardly explained just by T-induced change of the quasiparticle distribution function at the experimental [30] 15–20 K T difference, it should correspond to the characteristic order-parameter-induced spectral change.
[54] V. F. Elesin and Y. V. Kopaev, Phys. Usp. **24**, 116 (1981).
[55] J. T. Park, D. S. Inosov, A. Yaresko, S. Graser, D. L. Sun, P. Bourges, Y. Sidis, Y. Li, J.-H. Kim, D. Haug, A. Ivanov, K. Hradil, A. Schneidewind, P. Link, E. Faulhaber, I. Glavatskyy, C. T. Lin, B. Keimer, and V. Hinkov, Phys. Rev. B **82**, 134503 (2010).